

Postoperative intraocular lens tilt from preoperative full crystalline lens geometry using machine learning

EDUARDO MARTINEZ-ENRIQUEZ,^{*1} GONZALO VELARDE-RODRÍGUEZ,^{2,3} NICOLÁS ALEJANDRE-ALBA,^{2,3} DERICK ANSAH,⁴ SINDHU KISHORE,⁵ ÁLVARO DE LA PEÑA,¹ RAMYA NATARAJAN,^{6,7,8} PRAVIN VADDAVALLI,^{6,7,8} YUE ZHAO,⁹ JOSEPH O. OKUDOLO,⁴ DYLAN B. MCBEE,¹⁰ UGUR CELIK,⁴ MUJDAT CETIN,^{9,11} JEN-LI DONG,¹⁰ YULI LIM,¹⁰ LI WANG,¹⁰ DOUGLAS DONALD KOCH,¹⁰ SCOTT MACRAE,^{4,5} SUSANA MARCOS.^{4,5,12}

1. Instituto de Optica Daza de Valdes, Madrid, Comunidad de Madrid, Spain.
2. Ophthalmology Service, Fundación Jiménez Díaz University Hospital, Madrid, Spain.
3. Health Research Institute-Fundación Jiménez Díaz University Hospital, Universidad Autónoma de Madrid (IIS-FJD, UAM), 28040 Madrid, Spain.
4. Flaum Eye Institute, University of Rochester, Rochester, NY, United States.
5. Center for Visual Science, University of Rochester, Rochester, NY, United States.
6. Ophthalmic Biophysics, LV Prasad Eye Institute, Hyderabad, Telangana, India.
7. Cataract & Refractive Surgery Services, L V Prasad Eye Institute, Hyderabad, Telangana, India.
8. Shantilal Shanghvi Cornea Institute, L V Prasad Eye Institute, Hyderabad, Telangana, India.
9. Goergen Institute for Data Science & AI, University of Rochester, Rochester, NY, United States.
10. Department of Ophthalmology, Baylor College of Medicine, Houston, TX, United States.
11. Department of Electrical and Computer Engineering, University of Rochester, Rochester, NY, United States.
12. The Institute of Optics, University of Rochester, Rochester, NY, United States.

* eduardo.martinez@io.cfmac.csic.es

Abstract: In cataract surgery, the opacified crystalline lens is replaced by an artificial intraocular lens (IOL), requiring precise preoperative selection of parameters to optimize postoperative visual quality. Three-dimensional customized eye models, which can be constructed using quantitative data from anterior segment optical coherence tomography, provide a robust platform for virtual surgery. These models enable simulations and predictions of the optical outcomes for specific patients and selected IOL. A critical step in building these models is estimating the IOL's tilt and position preoperatively based on the available preoperative geometrical information (ocular parameters). In this study, we present a machine learning model that, for the first time, incorporates the full shape geometry of the crystalline lens as candidate input features to predict the postoperative IOL tilt. Furthermore, we identify the most relevant features for this prediction task. Our model demonstrates significantly lower estimation errors compared to a simple linear correlation method and a state-of-the-art approach that excludes full shape crystalline lens features, reducing the estimation error by approximately 5% compared to the latter. These findings highlight the potential of this approach to enhance the accuracy of postoperative predictions, paving the way to improve visual outcomes in cataract patients.

1. Introduction

Accurate quantification of anterior segment geometry in the human eye plays an important role in various clinical and surgical applications, such as cataract surgery planning, refractive surgery, contact lens fitting, and the diagnosis of corneal conditions such as keratoconus. Geometrical measurements of the cornea or/and crystalline lens have been reported using Placido ring-based systems [1], Purkinje imaging [2, 3], Scheimpflug imaging [1, 4, 5], ultrasound biomicroscopy [6], Magnetic Resonance Imaging [7, 8], and Optical Coherence Tomography (OCT) [9-11]. OCT, in particular, has gained popularity due to its high resolution, fast acquisition times, patient comfort, and wide clinical availability [12, 13]. It allows for the non-invasive visualization of both the cornea [11] and the crystalline lens [9, 10]. Once OCT images are corrected for fan, optical, and motion distortions, they provide the detailed structural data necessary for building three-dimensional (3-D) models of the anterior segment of the eye. These 3-D models enable clinicians to assess the impact of the shape of the ocular components and their relative alignment on the eye's optical quality. These evaluations are particularly valuable in understanding ocular conditions, such as myopia [14, 15], keratoconus [16], and the outcomes of cataract surgery [17-19].

The use of customized 3-D eye models has proven to be a significant advancement in the selection of intraocular lenses (IOLs) for cataract surgery, where the proper selection of IOL power is crucial for achieving optimal postoperative vision. One of the primary sources of error in IOL power calculations is the estimation of the IOL position (also known as the Estimated Lens Position (ELP), [20]). The complete quantification of the anterior segment, including the full geometry of the crystalline lens, has been shown to improve ELP predictions, leading to better surgical outcomes [17-19]. Beyond IOL position, IOL tilt and decentration are also relevant factors that could negatively impact the optical performance of the eye after cataract surgery, which may be particularly critical for specialized IOL designs such as aspheric, toric, or multifocal. Excessive amounts of tilt and decentration, generally resulting from a complicated surgery, can affect the visual quality by causing distortions, glare, and asymmetric optical aberrations. Increased tilt in a hinged haptic IOL platform, for example, has been associated with abnormal amount of coma [21, 22].

In addition to improving IOL power calculations, 3-D eye models offer a powerful tool for virtual surgery, enabling clinicians to simulate and predict the optical outcomes of cataract surgery with greater accuracy and precision [17]. These models integrate estimations of the IOL position and tilt, along with the geometric and optical properties of the IOL design, into the 3-D optical model of the eye. This enables the application of ray tracing, which simulates the passage of light through the eye, including the implanted IOL. Ray tracing facilitates the simulation of the optical degradation of the images projected on the retina for various powers of the same IOL model and for different IOL designs, such as aspheric, multifocal, and toric IOLs. By offering such detailed simulations, 3-D models can help clinicians to select the optimal IOL for individual patients, moving beyond the reliance on approximated formulas.

In earlier work, Rosales et al. and de Castro et al. [3, 23] used custom developed Purkinje imaging and/or Scheimpflug imaging, and Sun et al. [24] used a laboratory developed OCT to study the IOL tilt and decentrations in pseudophakic eyes. Recently, the use of images from commercial OCT-based systems, such as the IOLMaster 700 (Carl Zeiss Meditec, Germany), has allowed easier access to a much large number of patients and the study of the relationship between the tilt of the natural crystalline lens measured preoperatively and the postoperative IOL tilt in the same patients [25-28]. Firstly, Hirschschall et al. [26] studied the correlation between pre and postoperative tilt in 62 patients implanted with the same IOL. Then, Wang et al. [25] extended the work to 333 patients (65 pre and postoperatively), studying the repeatability, mirror symmetry between left and right eyes, and some correlations between tilt magnitude and ocular parameters, concluding that magnitude of crystalline lens tilt significantly increased with decreasing axial length and with increasing angle alpha. The

inverse correlation between crystalline lens tilt magnitude and axial length was also supported by Lu et al. [28] in a study on 131 emmetropic and 121 myopic eyes. Recently, Machine Learning (ML) models have been explored to study more complex relationships between preoperative ocular geometry and postoperative IOL tilt. In 2024, Waser et al. [27] presented a partial least squares regression and an ML approach to predict IOL tilt using preoperative biometry data in 50 eyes. This study concluded that the most important features for predicting the IOL tilt magnitude were preoperative tilt magnitude, pupil decentration, lens thickness and axial length.

The IOL is implanted within the capsular bag, and thus it is expected that the position and orientation of the IOL will be affected by the full size and shape of the crystalline lens as mechanical interactions between the capsular bag and the IOL haptics occur in the equatorial region of the bag. Nevertheless, none of the previous works have incorporated the full shape geometry of the crystalline lens as a potential factor influencing IOL tilt. Optical methods such as OCT obstruct views of the crystalline lens beyond the pupil margin and therefore the quantification is restricted to the visible area. Alternative methods allowing view of the full lens include ultrasound bio-microscopy and MRI, but these are less accessible in clinic than OCT, and require more cooperation from the patient and/or skill by the operator. We have previously presented a technique that allows realistic extrapolation of the crystalline lens full shape beyond the pupil, and a compact representation of this shape by the so-called *eigenlenses* [29-31]. The current study presents a method that applies machine learning algorithms to predict postoperative IOL tilt based on preoperative features in a large dataset of patients (476 eyes from 4 different sites and several IOL models implanted). The model includes, for the first time to the best of our knowledge, the information of the crystalline lens full shape. A large series of candidate input features (both geometrical and clinical) were considered, and the model analyzed their relative importance to improve the prediction. Then, we trained a specific tilt estimator using the selected features. We demonstrated that this method outperforms the estimation results from linear correlations and from the method proposed in [27], showing an improvement in overall performance.

2. Methods

2.1 Patients, surgery and clinical measurements

A total of 476 eyes from 346 patients (age mean \pm standard deviation = 70 ± 11 years old) were measured before and after standard cataract surgery (4.6 ± 4.7 months from surgery). Patients were implanted with one of the IOL models listed in Supplementary Table 1. The most frequently implanted IOLs were Acrysof (Alcon, $n=73$), Clareon (Alcon, $n=227$), enVista (B&L, $n=21$), Tecnis (J&J, $n=77$), Sensar (J&J, $n=10$), and FH5600 (Aurolab, $n=21$). The surgeries were performed at four different hospitals: 1) Flaum Eye Institute, University of Rochester, Rochester, NY, United States ($n=68$); 2) Department of Ophthalmology, Baylor College of Medicine, Houston, TX, United States ($n=115$); 3) Ophthalmology Department, Fundación Jiménez Díaz University Hospital, Madrid, Spain ($n=200$); 4) LV Prasad Eye Institute, Hyderabad, India ($n=93$). IOL power implanted ranged from +36 D to -5 D.

The final sample for the study included 356 eyes from 259 patients (age mean \pm standard deviation = 70 ± 11 years old, ranging from 24 to 92 years old; preoperative spherical equivalent mean \pm standard deviation = -0.80 ± 3.51 D, ranging from -26 D to 9 D).

From the initial 476 measured eyes, images from 8 eyes were not useful (mostly because the posterior surface of the crystalline lens or the IOL surfaces were not visible) and thus were discarded. Also, 4 eyes were discarded because of lack of compliance of full crystalline lens shape estimation and 3-D model construction (see Section 2.4 for details on model construction and full shape estimation). Additionally, measurements with pupils smaller than 3 mm were discarded ($n=96$). The reason of discarding eyes with small pupils is discussed the Discussion

Section. Finally, from the remaining 368 eyes, 12 eyes were discarded because they were considered outliers in the correlations and/or polar plots shown in Sections 3.1 and 3.2. Some possible clinical reasons for being outliers are discussed in the Discussion Section. Our analysis was thus performed on 356 eyes from 259 patients.

The study met the tenets of the Declaration of Helsinki. Ethical approval was granted by the Ethics Committee of Consejo Superior de Investigaciones Científicas (CSIC), Fundación Jiménez Díaz, University of Rochester Medical Center, Baylor College of Medicine, and LV Prasad Eye Institute. Written informed consent was obtained from the patients after detailed explanation of the procedure.

2.2 Overview of the solution

Figure 1 shows a schematic diagram of the methodology to estimate the postoperative (IOL) tilt from preoperative features. 3-D geometrical models are constructed from the preoperative OCT images of the patient's eye, including the full shape of the crystalline lens obtained with our proposed *eigenlenses* method [30, 31]. Geometrical features are obtained from these 3-D models (quantification), which along with clinical features, feed a Feature Selection and Machine Learning algorithm.

Similarly, 3-D models are constructed from the postoperative OCT images of the same patients, and the IOL tilt is measured (magnitude and direction, as defined in [26] and in Section 2.5). Postoperative tilt is used as ground truth in training the machine learning algorithm.

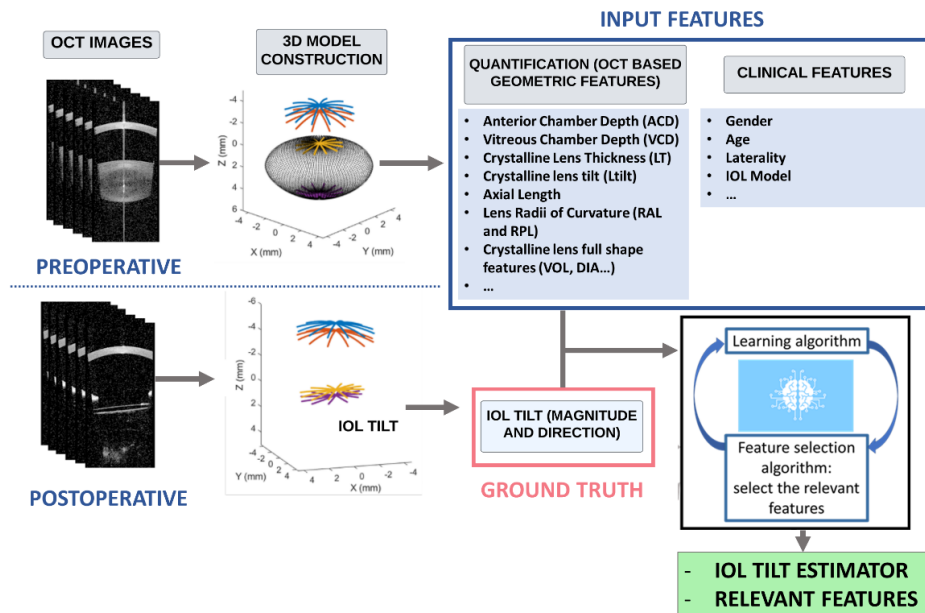


Fig. 1. Flow chart of the methodology to estimate the IOL tilt from preoperative measurements, that includes the 3-D model construction, quantification (for obtaining the geometrical features and the ground truth that will feed the machine learning algorithm) and feature selection/learning processes.

In the 3-D model construction, the anterior surface of the cornea (blue), posterior surface of the cornea (red), anterior surface of the crystalline lens/IOL (yellow), and posterior surface of the crystalline lens/IOL (purple) are represented. In the preoperative models, the full shape of the crystalline lens is also shown (black).

2.3 Optical coherence tomography imaging

OCT images of the anterior segment of the eye were acquired before and after cataract surgery with a commercial swept-source OCT system, the IOLMaster 700 (Carl Zeiss Meditec AG, Jena, Germany). The IOLMaster 700 operates at a speed of 2000 A-scans/s, at 1055 nm, with a 44.0 mm scan depth and 22 μm axial resolution in tissue [26, 32]. The horizontal scanning range is 6 mm. The IOLMaster 700 acquires six meridional B-scans at 30-deg steps, thus providing 3-D information. Figure 2 shows examples of cross-sectional meridians of the eye of a patient before (top) and after (bottom) the surgery.

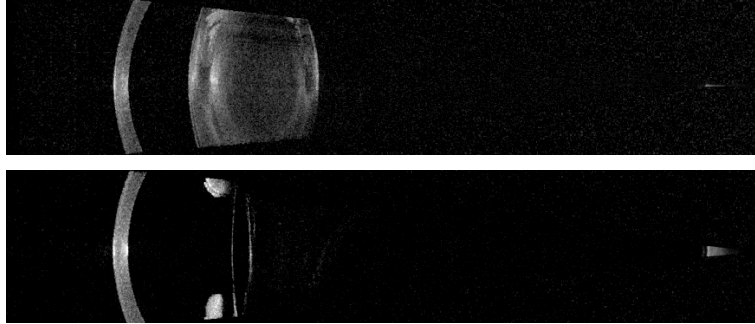


Fig. 2. Preoperative (top) and postoperative (bottom) IOLMaster 700 OCT images (meridian at 300°, OD, Female, 90 years old), showing the crystalline lens and the implanted IOL (Clareon CNA0T0 by Alcon, 23.5 D) respectively.

2.4 3-D eye model construction

Figure 3 illustrates the process to obtain the 3-D eye models from the OCT images, which involves [33]: (1) preprocessing of the images and automatic segmentation of the surfaces of interest (i.e., anterior and posterior surfaces of the cornea and crystalline lens and retina), using our deep learning segmentation algorithm proposed in [33]; (2) 3-D model construction, including conversion from pixels to millimeters using calibration data, correction of the optical distortion, and registration, transforming the data from the six meridians into a single coordinate system to obtain the 3-D model within the pupil; (3) crystalline lens full shape estimation from data corresponding to the central part visible through the pupil, using the *eigenlenses* method [30, 31] (only for preoperative measurements). Briefly, *eigenlenses* represent the most common “deformation patterns” that can be found in a training set of 133 isolated crystalline lenses, with respect to the average lens shape. Thanks to the richness of the training set (that includes lenses of ages ranging from 0 to 71 y/o), *eigenlenses* can represent efficiently the human crystalline lens shapes that can be found in nature. The first *eigenlens* (weighted by the a_1 coefficient, the most “common” deformation) describes changes in the size of the lens, while the second *eigenlens* (a_2 coefficient) describes changes in the aspect ratio (i.e., lenses more “stretched” or rounded). The third and fourth *eigenlenses* ($a_3 - a_4$ coefficients) are related with asymmetric changes in X or Y directions, and the fifth and sixth ($a_5 - a_6$ coefficients) with fine changes in the shape of the surfaces. The *eigenlenses* representation is compact, needing only 6 coefficients ($a_1 - a_6$) to capture 96% of the variance in shape of the training set of lenses. Thanks to this compaction ability, *eigenlenses* are useful to estimate the full shape of the lens in vivo from its central part visible through the pupil [30, 31].

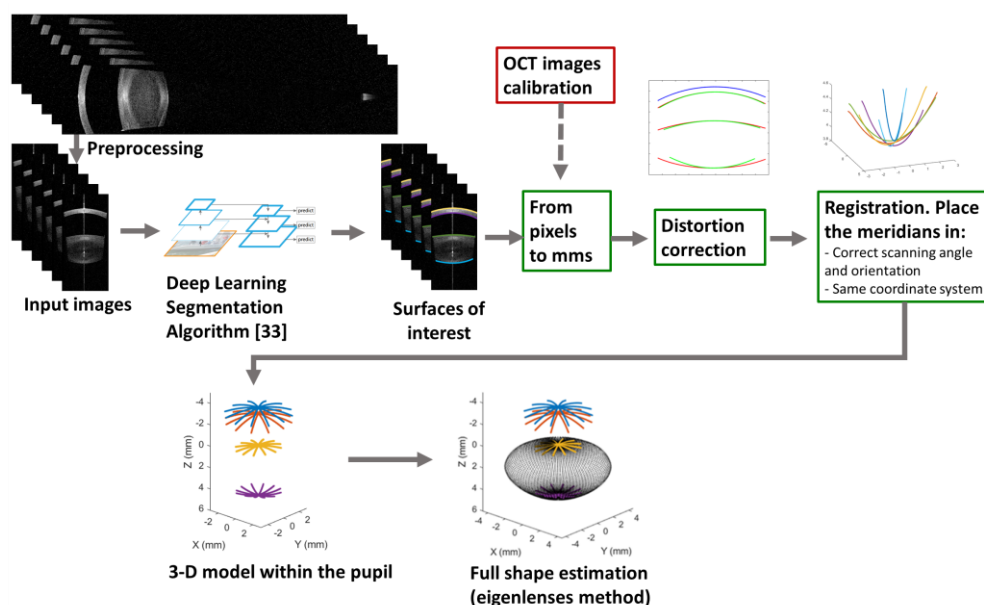


Fig. 3. Preoperative 3-D eye model construction. Surface segmentation, distortion correction, and registration were performed to generate 3-D models of the eye. The full shape of the crystalline lens was estimated using the *eigenlenses* method [30, 31]. The processes for obtaining 3-D postoperative models are the same, excluding the full shape estimation of the crystalline lens.

Although the analysis is performed automatically, for quality control purposes, the OCT images, the segmentation process and the final retrieved 3-D models were visualized by two different trained observers, who checked that the images had sufficient quality, that all the surfaces of interest were visible, that they were correctly detected by the algorithm, and that the 3-D models were smooth, ensuring that all automatic processes were carried out correctly.

2.5 Quantification

The quantification process involves measuring the geometrical features from the preoperative 3-D models which are used, along with the clinical features, as input features that feed the machine learning and feature selection algorithms. Also, the quantification of the IOL tilt from postoperative 3-D models is used as ground truth.

2.5.1 Input features

From the 3-D model of each eye we measured 65 features. Specifically, the set of features included (see Supplementary Appendix 1 for a brief description of each feature and its corresponding acronym):

- *Preoperative clinical and IOLMaster 700 features*: 16 features obtained in the clinic or directly output by the IOLMaster 700, including patient age, gender, laterality of the eye, preoperative refraction (Sphere, Cylinder, Spherical equivalent), IOL model and power implanted, axial length, pupil size, and keratometry.

- *Preoperative geometrical features obtained from OCT (3-D models within the pupil)*: 25 geometric features of the eye obtained directly from OCT images. Specifically, these features are quantified from the 3-D models considering only the part of the crystalline lens that is visible throughout the pupil (before estimating the full shape of the crystalline lens) using

custom developed algorithms that have been successfully applied to custom designed and commercial OCT systems in our prior work [33, 34]. Measured parameters include axial distances and curvatures of the different surfaces within the eye (anterior and posterior cornea and crystalline lens), and preoperative tilt (magnitude and direction) of the crystalline lens. Preoperative tilt is defined as explained in Section 2.3.2 for the IOL. Radii of curvatures were calculated searching the best fitting sphere in a fitting area of 6 and 3 mm (see supplementary document for details).

- *Preoperative crystalline lens full shape features obtained from OCT*: 24 features related with the crystalline lens full shape, such as its volume, equatorial plane position or its diameter (estimated as in [9, 29, 30]), and the coefficients of the *eigenlenses* method. The *eigenlenses* and *eigencenter* coefficients (*eigenlenses* constructed to represent the optical zone of the crystalline lens that is visible through the pupil) were determined in accordance with [30, 31]. These features were of special interest and introduced in the current study for the first time.

Figure 4 illustrates the definition of some of these features.

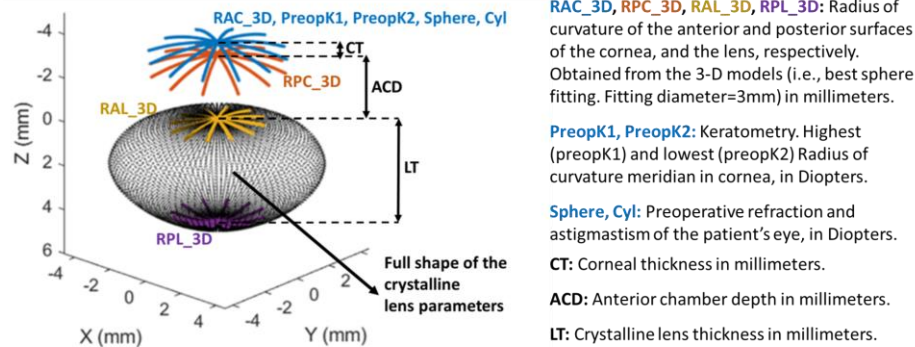


Fig. 4. Definition of some of the features from 3-D preoperative models.

2.5.2 Ground truth

The ground truths for the variables to be predicted (IOL tilt magnitude and IOL tilt direction) were obtained from the postoperative models. These variables are defined in Figure 5 and are described in detail in earlier work [26]. The tilt was obtained by: (1) calculating the middle plane between the anterior and posterior surfaces of the IOL using multiple linear regression; (2) obtaining the normal vector to that middle plane; (3) calculating the angles (tilt magnitude, polar angle in spherical coordinates; and tilt direction, azimuthal angle in spherical coordinates) as defined in Figure 5. Intuitively, tilt magnitude indicates the “amount” of tilt, and tilt direction indicates the “orientation” of that tilt. Tilt direction ranges from $[0^\circ, 180^\circ] \cup (0 \text{ to } -180^\circ)$ and tilt magnitude from 0 to 9° (maximum value found in the data set). The same definitions apply to preoperative tilt of the natural crystalline lens.

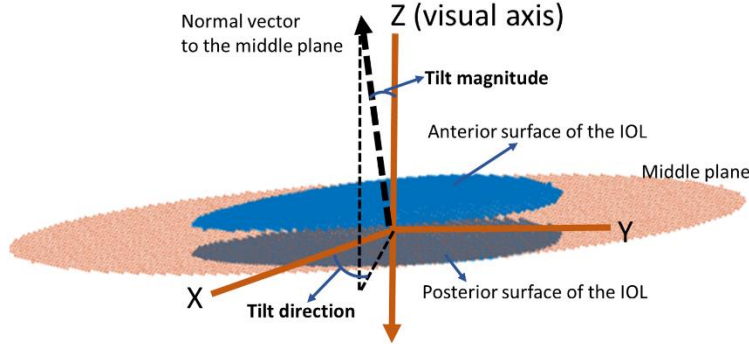


Fig. 5: Definition of the IOL tilt magnitude and direction from the 3-D postoperative models. These are the variables to be predicted.

2.6 Feature selection and estimation

Two estimators were designed using ML approaches for the estimation of the IOL tilt magnitude and direction. Several regression methods were tested, in particular ridge models, regression trees, support vector machines, Gaussian process regression (GPR), ensembles of trees, and neural networks. In both estimation problems (estimation of tilt magnitude and of direction) GPR provided the minimum estimation error across methods, and thus, the results using GPR are reported in this study. A 5-fold cross-validation approach was used (i.e., splitting the sample in 5 groups, using 4 for training and 1 for test) and the experiments were repeated 100 times. The optimization metric was the average across experiments of the mean absolute error (MAE) in degrees between estimated and actual lens tilt (magnitude and direction) in the test set.

The relevant features were selected using a sequential forward feature selection algorithm that starts with an empty set of features and, in each iteration of the algorithm, selects the feature that, in combination with the set of features already selected, minimizes the estimation error using a GPR method ([35-37]). The algorithm stops if the MAE does not decrease when a new feature is added (i.e., if there is no improvement in prediction).

For the definition of GPR, we considered the following model [35-37]:

$$g(\mathbf{x}) = f(\mathbf{x}) + \mathbf{h}(\mathbf{x})^T \boldsymbol{\beta}$$

where $f(\mathbf{x})$ is a zero mean Gaussian Process, $f(\mathbf{x}) \sim GP(0, k(\mathbf{x}, \mathbf{x}'))$, $\mathbf{h}(\mathbf{x})$ are a set of fixed basis functions that transform the original feature vector \mathbf{x} , and $\boldsymbol{\beta}$ are basis function coefficients.

In our experiments, we chose a constant basis function $\mathbf{h}(\mathbf{x})$ and an exponential kernel, defined as follows:

$$k(x_i x_j | \boldsymbol{\theta}) = \sigma_f^2 \exp\left(-\frac{r}{\sigma_l}\right)$$

where σ_l is the characteristic length scale and $r = \sqrt{(x_i - x_j)^T (x_i - x_j)}$ is the Euclidean distance between x_i and x_j . Thus, the model is completely defined by the variance of noise σ_n^2 , the $\boldsymbol{\beta}$ coefficients, and the hyperparameters of the kernel function σ_f and σ_l , which are obtained by

training the model, and are specified in the results section for each estimator. Features are standardized (centering data around the mean and scaling to the standard deviation) to train the algorithm.

2.7. Data analysis

Linear regression analysis between preoperative and postoperative tilt magnitude and direction, and between left and right eyes was performed, obtaining the Pearson correlation coefficient (r), the p -value for testing the hypothesis of no correlation, and 95% confidence intervals (related with the regression line) over the regression parameters.

We compared the mean value across experiments of MAE for consecutive number of features in the feature selection algorithm using a two-tailed paired t -test. We also compared the mean MAE across experiments using different estimation methods (linear correlation, [27] and the proposed method) using a two-tailed paired t -test with Bonferroni correction. The normality of the MAE data distribution was assessed with the Kolmogorov-Smirnov test.

For all analyses, statistical significance was defined as a p -value lower than 0.05. Calculations were performed with Matlab (MathWorks, Natick, MA, USA, version R2022b).

3. Results

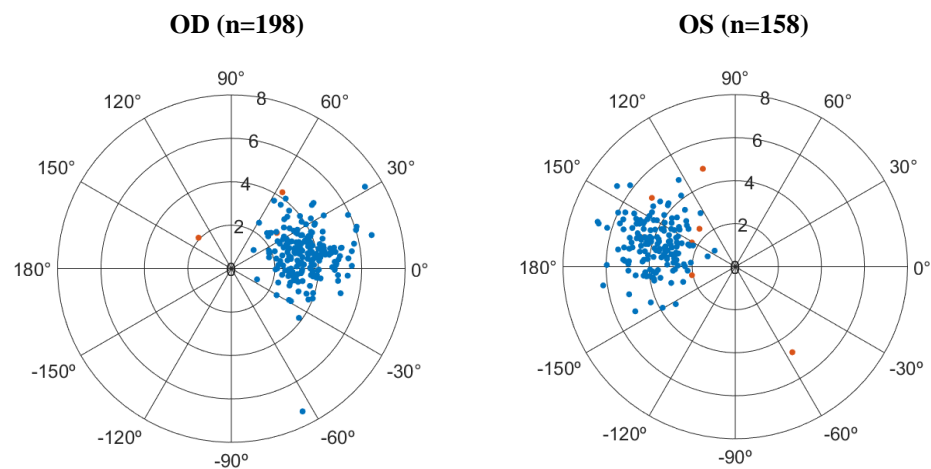
In this section we (1) analyze the tilt magnitude and direction in right and left eyes and the correlation between tilt pre and postoperatively, and between right and left eyes; (2) show the ranking of features that best estimate tilt magnitude and direction (feature selection); (3) present the results obtained with an estimator trained with the best set of selected features.

3.1 Tilt magnitude and direction in right and left eyes

Figure 6 shows polar plots that represent the preoperative (crystalline lens) and postoperative (IOL) tilt magnitude and direction for right and left eyes. Following the representation proposed in earlier work [25], the radial distance to the center (from 0° to 8° in preoperative and from 0° to 11° in postoperative) represents the tilt magnitude in degrees, while the angle represents de tilt direction ($[0^\circ, 180^\circ] \cup (0 \text{ to } -180^\circ)$).

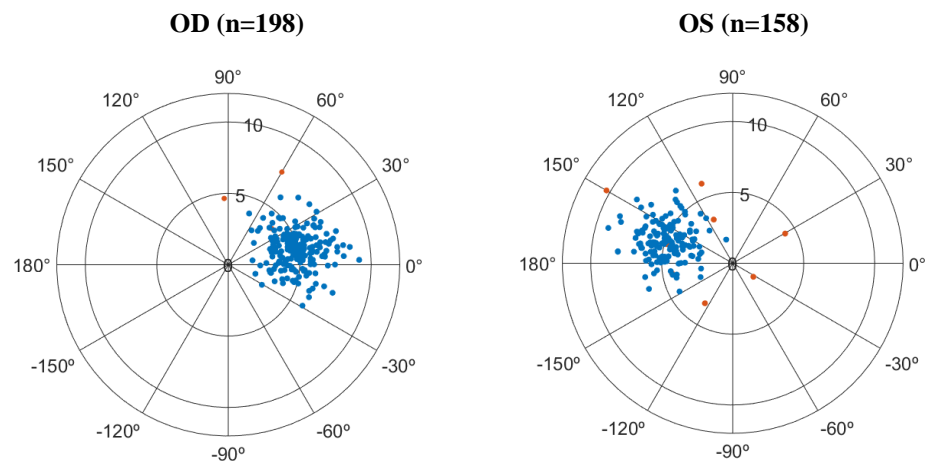
Preoperatively, the mean \pm STD crystalline lens tilt magnitude was $3.63^\circ \pm 1.00^\circ$ and $3.98^\circ \pm 1.03^\circ$ for OD and OS respectively, tilted nasally for both eyes (tilt direction of $10.97^\circ \pm 17.70^\circ$ and $164.22^\circ \pm 16.08^\circ$ respectively). Postoperatively, the IOL tilt magnitude was $5.06^\circ \pm 1.30^\circ$ and $5.12^\circ \pm 1.36^\circ$ for OD and OS respectively, tilted nasally for both eyes (tilt direction of $13.14^\circ \pm 16.68^\circ$ and $161.50^\circ \pm 15.81^\circ$).

Preoperative (crystalline lens)



A)

Postoperative (IOL)



B)

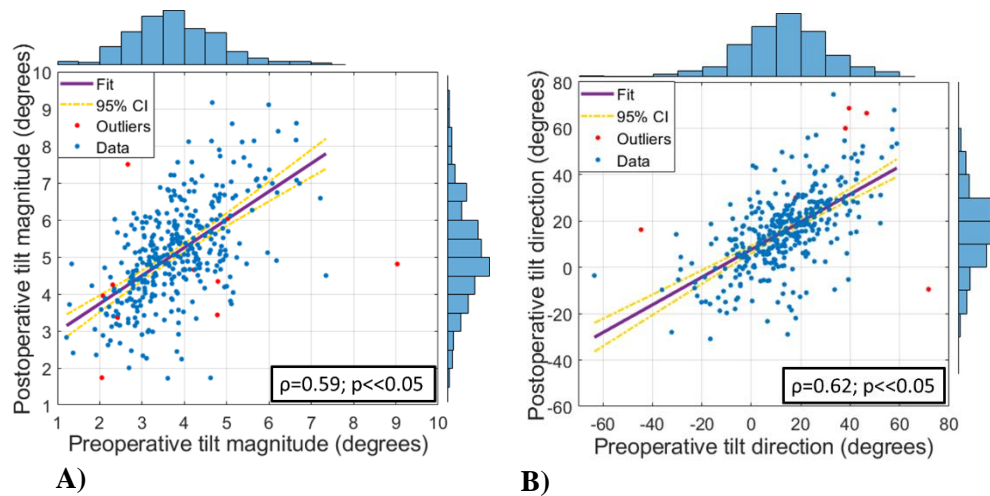
Fig. 6: Polar plots for right (left column) and left (right column) eyes, where the radial distance to the center represents the tilt magnitude in degrees, while the angle represents the tilt direction. A) Preoperative natural crystalline lens tilt; B) Postoperative IOL tilt. Outliers are shown in red.

3.2 Correlation between pre- and postoperative tilt and between right and left eyes

Figure 7 shows the correlation between preoperative and postoperative tilt magnitude (Fig 7A) and direction (Fig 7B). Pearson correlation coefficients (ρ) and the p-value for testing the hypothesis of no correlation are shown. Marginal histograms, 95% confidence intervals and best linear model are also presented in Figure 7.

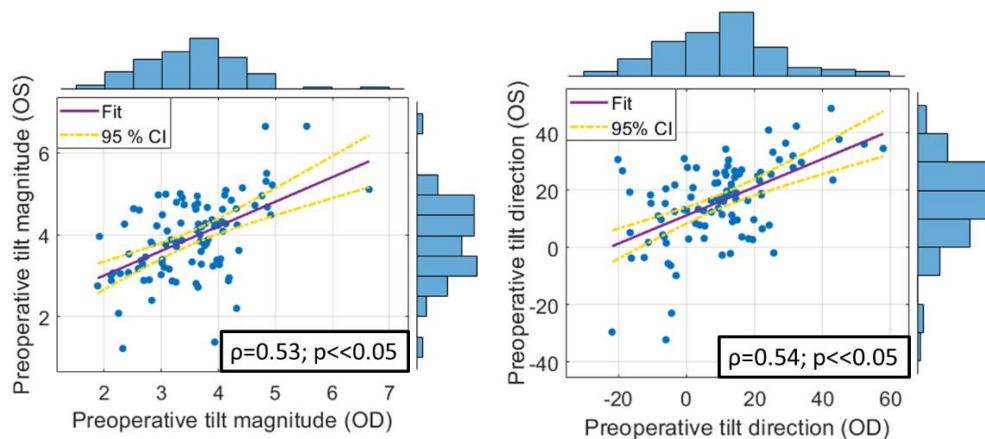
399 Note that, in this case, to obtain meaningful correlations, left eyes were reflected (i.e., tilt
400 direction was changed) as follows:

401
402 $\text{if } \text{tilt}_{\text{direction}} \geq 0 \rightarrow \text{tilt}_{\text{direction}} = 180 - \text{tilt}_{\text{direction}}$
403 $\text{elseif } \text{tilt}_{\text{direction}} < 0 \rightarrow \text{tilt}_{\text{direction}} = -180 - \text{tilt}_{\text{direction}}$
404



405
406 Fig. 7: Scatterplot with best linear regression lines, marginal histograms, and 95% confidence intervals (CI) between
407 preoperative tilt (the tilt of the natural crystalline lens before the surgery) and postoperative tilt (the tilt of the IOL
408 implanted). A) Tilt magnitude. B) Tilt direction. Pearson correlation coefficients (ρ) and the p-value for testing the
409 hypothesis of no correlation are also shown. Outliers (not taken into account for fitting the model) are shown in red
410 color (some outliers are not visible because they are out of the range represented in the axes).
411

412 Figure 8 shows the correlation between right eyes (OD) and left eyes (OS) for preoperative (top row)
413 and postoperative (bottom row) tilt magnitude (Fig 8A, left column) and direction (Fig 8B, right column). A total of 97 patients with paired eyes were used in the analysis. Pearson
414 correlation coefficients (ρ) and the p-value for testing the hypothesis of no correlation are shown. Marginal histograms, 95% confidence intervals and best linear model are also
415 represented.
416
417
418



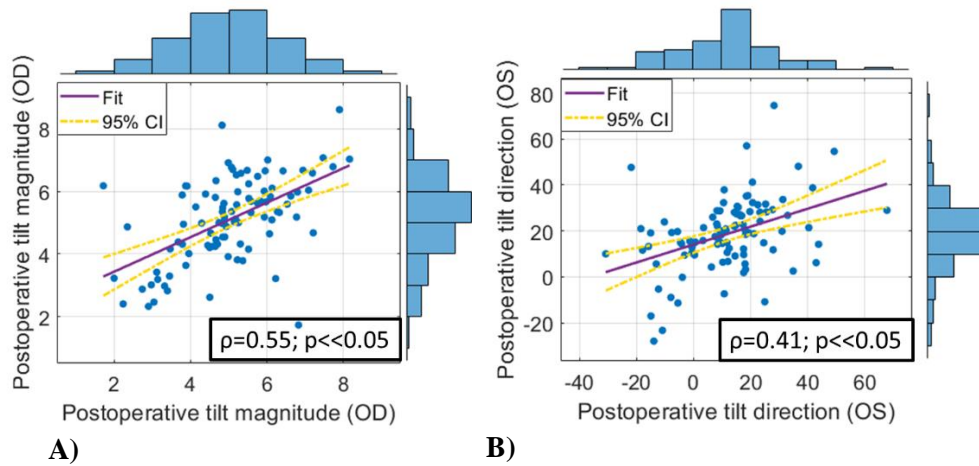


Fig. 8: Scatterplot with best linear regression lines, marginal histograms, and 95% confidence intervals (CI) between right eyes (OD) and left eyes (OS). Top row: preoperative measurements; bottom row: postoperative measurements. A) Tilt magnitude; B) Tilt direction. 97 patients with paired eyes are used in the analysis. Pearson correlation coefficients (ρ) and the p-value for testing the hypothesis of no correlation are also shown.

3.3 Feature selection

Figure 9 shows the decrease in estimation error as we are including the features selected by the feature selection algorithm (the order indicates the feature ranking). Error bars represent STD across experiments and asterisks indicate statistically significant differences between mean MAE for consecutive number of features. From the 65 candidate features, there were six that were consistently identified across experiments by the feature selection algorithm as the primary features to predict IOL tilt magnitude and direction (i.e., inclusion of a higher number of features did not produce a decrease in MAE).

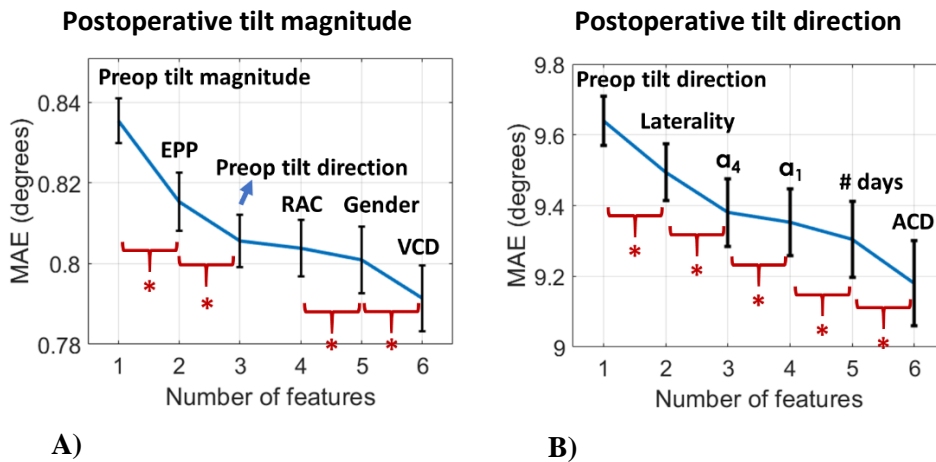


Fig. 9: Feature selection process, quantifying the decrease of MSE as new features are included in the estimation. A) Postoperative tilt magnitude estimation. The ranking of Features is: 1) Preoperative tilt magnitude; 2) Equatorial Plane Position (EPP), obtained from the full shape of the crystalline lens; 3) Preoperative tilt direction; 4) Radius of curvature of anterior cornea (RAC); 5) Gender; 6) Vitreous Chamber Depth (VCD); B) Postoperative tilt direction estimation. The ranking of features is: 1) Preoperative tilt direction; 2) Laterality of the eye (OD-OS); 3) α_4 eigenlens coefficient, that indicates asymmetric changes of the shape of the lens; 4) α_1 eigenlens coefficient, related with the

size of the crystalline lens; 5) # days (Number of days since operation, defined as the number of days from surgery to postoperative scan); 6) ACD (Anterior Chamber Depth). Error bars represent STD across experiments. Asterisks indicate statistically significant difference between mean MAE for consecutive number of features (i.e., comparing consecutive states of the feature selection algorithm). Paired t-test, $p < 0.05$.

Table 1 shows the mean, STD, maximum and minimum values of the selected features for the tilt magnitude and direction estimations.

Table 1. Summary of the selected features.

Magnitude	Preop tilt Magnitude (degrees)	EPP (mm)	Preop tilt Direction (degrees)	RAC (mm)	Gender (M/F)	VCD (mm)
Mean \pm STD	3.78 \pm 1.03	2.01 \pm 0.25	13.1 \pm 17.15	7.86 \pm 0.31	149/207	15.86 \pm 1.21
Range (Min./Max.)	1.21/7.35	1.34/2.63	-63.5/58.85	6.59/9.53	--	12.65/24.47

Direction	Preop tilt Direction (degrees)	Laterality (OD/OS)	a_4	a_1	# days (days)	ACD (mm)
Mean \pm STD	13.1 \pm 17.15	198/158	0.97 \pm 0.53	-2.7 \pm 18.4	140 \pm 141	2.58 \pm 0.38
Range (Min./Max.)	-63.5/58.8	--	-0.51/3.20	-68/43	6/586	1.58/3.59

STD, Standard deviation; EPP, Equatorial plane position; RAC, Radius of curvature of anterior cornea; VCD, Vitreous chamber depth; # days, Number of days since operation; ACD, Anterior chamber depth

3.4 Estimation error and optimal parameters in training

Table 2 shows the mean absolute error (MAE, in degrees) \pm STD of the estimation, the eye with maximum estimation error (Max. error) and the number of eyes with estimation error higher than MAE $+\sigma$, where σ is one standard deviation across eyes (approximately 1.5 degree for the tilt magnitude and 17 degrees for the tilt direction). Linear correlation model (correlation shown in Figure 7), GPR estimation algorithm trained using the features proposed in Waser et al. [27] (only for tilt magnitude), and the proposed algorithm using the features described in the previous section are compared. Note that for comparisons with [27] we used the preoperative tilt magnitude, lens thickness, and axial length as suggested in the paper, but we were not able to include pupil decentration as feature because we did not have that value for all the eyes. The last column indicates the p-value for testing the difference between means (paired t-test with Bonferroni correction). The second row shows the MAE for the estimation of the postoperative magnitude and the third row for the estimation of the postoperative direction. The STD is calculated across experiments, and the linear correlation model was included in the cross-validation loop (i.e., the MAE results were obtained in a test set not used to obtain the linear model).

Table 2. Mean MAE \pm STD across experiments (degrees), maximum estimation error (Max. error) and number of eyes with estimation error higher than 1.5/ 17 degrees (magnitude/ direction respectively). Linear correlation model, a method trained with the features proposed in [27] (except for pupil decentration) and the proposed algorithm are compared.

	Results	Linear correlation	[27]	Proposed	p-value
Postoperative tilt magnitude	MAE (deg.)	0.84 \pm 0.003	0.83 \pm 0.007	0.79 \pm 0.007	$p < 0.05$
	Max. error (deg.)	4.00	4.23	3.97	
	Error > 1.5 degrees	61	56	48	

Postoperative tilt direction	MAE	9.60±0.04	---	9.18±0.11	p<<0.05
	Max. error (deg.)	47.5	---	46	
	Error>17 degrees	58	---	55	

The application of the proposed method results in both lower errors (decreased MAE) and in a lower number of eyes with high errors in comparison with linear correlation and [27]. STD of the MAE of tilt magnitude across eyes was marginally lower for the new method: 0.69 deg, 0.69 deg, and 0.68 deg for linear correlation, [27], and proposed methods respectively. STD of the MAE of tilt direction was also lower for the proposed method: 8.80 degrees and 8.61 degrees for linear correlation and proposed respectively. These results suggest that the proposed estimator is more robust across different eyes.

Table 3 shows the optimal parameters selected for the GPR in the estimation of the tilt magnitude (first row) and tilt direction (second row).

Table 3. GPR optimal trained parameters for tilt magnitude and direction.

	σ_n	β	σ_f	σ_l
Postoperative tilt magnitude	0.86	5.0	1.61	9.24
Postoperative tilt direction	9.72	14.1	31.3	18.04

Variance of noise σ_n^2 , β coefficients, and hyperparameters of the kernel function σ_f and σ_l .

4. Discussion

The estimation of postoperative intraocular lens (IOL) tilt and position from preoperative measurements is a promising approach for enhancing the accuracy of cataract surgery optical predictions. By integrating these estimates into a virtual surgery tool, along with eye's and IOL geometrical values and estimates of the IOL position, it is possible to build custom eye models and simulate the optical quality by ray tracing. In this work, we propose a machine learning model designed to estimate IOL tilt. To our knowledge, this model is the first in the literature to utilize the full shape geometry of the crystalline lens as candidate input features, providing a more comprehensive representation of the eye's anatomical structure. We also focus on identifying the most relevant set of features to improve prediction accuracy and model efficiency for this task.

Mean tilt magnitude and direction obtained in this paper were similar to the ones reported in previous works using IOLMaster 700. Mean preoperative (crystalline lens) tilt magnitude was 3.8° in our work, 4.3° in [26], and 3.7° in [25], and postoperative (IOL) tilt magnitude was 5.1° in this paper, 6.2° in [26], and 4.9° (OD) and 5.2° (OS) in [25]. Mean preoperative tilt direction, after mirroring left eyes, was 13.1° in this work and 15.8° in [26]. Postoperative tilt direction was 15.5° in this work and 16.8° in [26]. Remarkably, postoperative tilt magnitude was higher than preoperative in all the results reported. Correlation coefficient between pre- and postoperative tilt magnitude was $\rho=0.59$ in this paper, $\rho=0.37$ in [26], and $\rho=0.70$ in [25]. The correlation between pre- and postoperative tilt direction was $\rho=0.62$ in this work, $\rho=0.71$ in [26], and $\rho=0.76$ in [25]. In this work we used data from 356 eyes measured pre and postoperatively to train the models, in comparison with 62 [26], 65 [25] and 50 [27] in previous work. The five times larger sample in the current work should largely contribute to the generalization ability of the machine learning algorithm.

Although the mean improvement on the estimation of 0.05 degrees in tilt magnitude and 0.4 degrees in tilt direction may not be clinically relevant, the significant reduction of eyes with large tilt estimation errors makes the approach potentially valuable in those individuals. We found that the number of eyes with MAE greater than 1.5 degrees in tilt magnitude is reduced by 13 eyes (from 61 to 48 eyes) by using our proposed method instead of linear correlation. Furthermore, the number of eyes with MAE greater than 17 degrees in tilt direction is reduced by 3 eyes (from 58 to 55 eyes). Previous work showed that the presence of physiological tilt compensated corneal lateral coma, rather than degrading the optics [38]. However, IOL tilt above a certain physiological amount can induce astigmatism and higher-order aberrations. Furthermore, to illustrate the extent to which the tilt magnitude and tilt direction affect the implantation axis of a toric lens, a wavefront simulation was conducted by Waser et al. with toric IOLs [27]. The study concluded that incorporating the consideration of postoperative IOL tilt into the preoperative calculations is associated with improved visual performance for the patient, particularly for those receiving toric lenses.

In our study, 96 eyes were excluded because their pupils measured less than 3 mm. This exclusion was based on two main considerations: (i) Reliability of geometric parameter estimation. The estimation of the full shape of the crystalline lens and other geometric parameters, such as radii of curvature is more reliable for larger pupils. As demonstrated before [39] the variance in certain geometric parameters for age-matched eyes increases significantly when pupils are smaller than 3 mm. Additionally, findings using donor lenses showed that the accuracy in estimating the full shape parameters, such as lens volume, improved for pupils larger than 3 mm, but the estimation was only slightly better with 5 mm-pupils compared to 4 mm pupils. (ii) Stability in calculating lens tilt. The calculation of the crystalline lens tilt is more reliable with pupils larger than 3 mm. For larger pupils, the orientation of mid-plane derived from the anterior and posterior lens surfaces is more stable, improving the accuracy of tilt measurements.

In our study, we excluded some outliers in the polar plots or pre/postoperative tilt correlations (12 eyes, marked in red in Figures 6 and 7). These eyes did not show small pupils, and OCT images and constructed 3-D models were apparently correct. Further analysis of these cases showed interocular axial length discrepancies postoperatively, steep corneal curvatures, interocular keratometry discrepancies, and eye fixation difficulties. Review of clinical history of some of these patients also showed some indications (capsular contraction syndrome, haptic dislocation, and intravitreal injections prior to the cataract surgery). The analysis of the potential relation between low predictability in those cases and clinical complications is beyond the scope of the current study.

During the feature selection process, six features were selected, corresponding to the mean number automatically selected by the feature selection algorithm across experiments. This number of features is considered appropriate relative to the sample size, helping to mitigate the risk of overfitting. Specifically, when estimating IOL tilt magnitude, the preoperative tilt magnitude was selected in 100% of the experiments, EPP in 95%, the preoperative tilt direction in 90%, gender in 70%, and RAC and VCD in 65% of the experiments. When estimating the IOL tilt direction, the preoperative tilt direction, laterality of the eye and a_4 *eigenlens* coefficient were chosen in 100%, number of days from surgery (# days) in 37%, a_1 coefficient in 28% and IOL model and ACD in 21%. Our analysis showed that for both magnitude and direction, the second and third features were the most effective in reducing estimation error, compared to using only the preoperative tilt. Additionally, the inclusion of the fourth feature (RAC for magnitude and a_1 coefficient for direction) resulted in only a slight reduction in MAE. Notably, when the fourth feature was excluded, adding the remaining features (fourth to sixth) did not further improve estimation accuracy. This suggests that the observed reduction

in MAE after the third feature is primarily driven by the interaction between the fourth, fifth, and sixth features. Importantly, all reductions in MAE associated with the inclusion of additional features were statistically significant except for the case of RAC (from the third to fourth order feature in magnitude estimation).

As expected, the preoperative tilt of the crystalline lens was the most important feature for predicting IOL tilt. Significantly, geometrical features describing the full shape of the crystalline lens are selected for the estimation of the magnitude (EPP) and direction (coefficients a_4 and a_1). EPP, defined as the distance between the anterior surface apex and the equator of the crystalline lens, is only available through the estimation of the full shape of the lens. In good agreement with other studies [25, 27, 28] we also found a significant correlation between axial length (AL) and IOL tilt magnitude ($\rho=-0.25$, $p<<0.05$). Nevertheless, AL is not selected by the feature selection algorithm, probably because this information is already explained by the preoperative tilt magnitude and the EPP, also correlated with AL. Our earlier work in a young subject cohort of crystalline lens parameters as a function of myopia found correlations between AL and EPP, with longer eyes showing lower EPP [14]. However, the selection of EPP as a primary feature indicates that EPP provides complementary information to estimate the tilt in a non-linear fashion. This relationship may stem from the fact that lower EPPs are typically associated with more elliptical crystalline lens shapes, whereas higher EPPs correspond to more rounded lens shapes. In cases with more rounded lens shapes, the intraocular lens (IOL) may not fit as well, leading to a lower tilt magnitude. For tilt direction, it is reasonable that “non-symmetric” features play a more critical role. In the current study we observed a statistically significant difference for preoperative tilt magnitude and direction as well as postoperative tilt direction between right and left eyes (after mirroring left eyes), t-test, $p<<0.05$. Similar findings were previously reported [27], and may explain the importance of laterality in improving prediction accuracy. Additionally, the *eigenlens* coefficient a_4 was identified as an important feature, reflecting asymmetric changes in lens shape after removing tilt. This asymmetry intuitively influences the tilt direction. Some features, such as RAC, are less intuitive, but they may contribute through non-linear interactions with other features, providing complementary information to enhance predictions.

In our training, we used pairs of correlated eyes (OD-OS). Although it is generally recommended to either include both eyes from a pair in the same set (training or testing) or use one eye per pair to minimize the risk of overfitting, we found minimal variation in estimation error across cross-validation folds and experiments that have different proportions of randomly selected OD-OS pairs (STD across experiments of 0.007 and 0.11 degrees for tilt magnitude and direction respectively). These results indicate that overfitting is not a concern and that the inclusion of eye pairs does not adversely affect the outcomes.

Our trained model can be used to predict IOL tilt based on preoperative OCT imaging, or new models can be trained that are specific, for example, to a specific IOL type. A similar strategy can be applied to estimate the position of the IOL from some preoperative OCT geometrical features [39]. Therefore, the computational cost to extract the required geometrical features for applying the algorithm would also serve the purpose of estimating the ELP, obtaining all the necessary data for the construction of the 3-D model that would be used as input to the virtual surgery platform. Remarkably, the procedure can be applied on the OCT scans that are routinely acquired preoperatively for biometry measurements (in this case using the IOLMaster700) that are standard of care in many practices.

5. Conclusion

We have proposed a method for the IOL tilt estimation after cataract surgery from preoperative features of each patient, including, for the first time, geometrical features of the full shape of the crystalline lens. This is useful to create a virtual surgery platform. By integrating these advanced prediction methods into clinical practice, surgeons can potentially select the most appropriate IOL for each patient, reducing the risks associated with IOL misalignment, improving long-term outcomes, and ultimately providing better visual quality for patients after cataract surgery.

In the future, we plan to explore several open interesting questions regarding the factors influencing IOL tilt that could be solved with our data set, including: (i) How do factors such as the surgeon's technique or the clinical site impact IOL tilt? (ii) Does the choice of IOL model affect tilt and its prediction? (iii) Are certain features more important for predicting IOL tilt in different IOL models? (iv) Is there an improvement in accuracy by training each IOL model separately? Additionally, it will be valuable to investigate tilt in toric lenses, as well as examine the relationship between IOL tilt and other visual quality metrics and clinical features, such as cataract grade.

Funding. Project supported in part by a 2023 Leonardo Grant for Researchers and Cultural Creators, BBVA Foundation; Supported in part by RYC2022-038195-I, MCIN/AEI and FSE+; Spanish Government grant PID2023-152641OA-I00; Autonomous Community of Madrid (CAM) grant TEC-2024-COM-322; NIH/NEI Grant EY035009; NIH/NEI P30 Core Grant EY001319-46; Empire State Development Funds- Center of Excellence in Data Science Grant; Spanish government grant PID2020-115191 RB-I00; Unrestricted grant from Research to Prevent Blindness to the University of Rochester Department of Ophthalmology and Department of Ophthalmology at Baylor College of Medicine; SRB Charitable Corp., Fort Worth, TX, and the Sid W. Richardson Foundation, Fort Worth, TX.

Disclosures. EME (P), SM (P).

Data availability. Data underlying the results presented in this paper are available in the "Postoperative-intraocular-lens-tilt-from-preoperative-full-crystalline-lens-geometry" repository, [40].

Supplemental document. See Supplement 1 for supporting content.

References

- [1] S. A. Read, M. J. Collins, D. R. Iskander, and B. A. Davis, "Corneal topography with Scheimpflug imaging and videokeratography: comparative study of normal eyes," (in eng), *J Cataract Refract Surg*, vol. 35, no. 6, pp. 1072-81, Jun 2009, doi: 10.1016/j.jcrs.2009.01.020.
- [2] P. Rosales, M. Dubbelman, S. Marcos, and R. van der Heijde, "Crystalline lens radii of curvature from Purkinje and Scheimpflug imaging," *J Vis*, vol. 6, no. 10, pp. 1057-67, Sep 19 2006, doi: 10.1167/6.10.5.
- [3] P. Rosales and S. Marcos, "Phakometry and lens tilt and decentration using a custom-developed Purkinje imaging apparatus: validation and measurements," *J Opt Soc Am A Opt Image Sci Vis*, vol. 23, no. 3, pp. 509-20, Mar 2006. [Online]. Available: <http://www.ncbi.nlm.nih.gov/pubmed/16539046>.
- [4] M. Dubbelman, G. L. Van der Heijde, and H. A. Weeber, "Change in shape of the aging human crystalline lens with accommodation," *Vision Res*, vol. 45, no. 1, pp. 117-32, Jan 2005, doi: 10.1016/j.visres.2004.07.032.
- [5] C. A. Cook, J. F. Koretz, A. Pfahnl, J. Hyun, and P. L. Kaufman, "Aging of the human crystalline lens and anterior segment," *Vision Res*, vol. 34, no. 22, pp. 2945-54, Nov 1994, doi: 10.1016/0042-6989(94)90266-6.
- [6] V. Ramasubramanian and A. Glasser, "Objective measurement of accommodative biometric changes using ultrasound biomicroscopy," *J Cataract Refract Surg*, vol. 41, no. 3, pp. 511-26, Mar 2015, doi: 10.1016/j.jcrs.2014.08.033.

678 [7] D. A. Atchison, E. L. Markwell, S. Kasthurirangan, J. M. Pope, G. Smith, and P. G. Swann, "Age-related
679 changes in optical and biometric characteristics of emmetropic eyes," *J Vis*, vol. 8, no. 4, pp. 29 1-20, 2008,
680 doi: 10.1167/8.4.29.

681 [8] S. Kasthurirangan, E. L. Markwell, D. A. Atchison, and J. M. Pope, "MRI study of the changes in crystalline
682 lens shape with accommodation and aging in humans," *J Vis*, vol. 11, no. 3, 2011, doi: 10.1167/11.3.19.

683 [9] E. Martínez-Enriquez, P. Perez-Merino, M. Velasco-Ocana, and S. Marcos, "OCT-based full crystalline
684 lens shape change during accommodation in vivo," *Biomed Opt Express*, vol. 8, no. 2, pp. 918-933, Feb 01
685 2017, doi: 10.1364/BOE.8.000918.

686 [10] P. Perez-Merino, M. Velasco-Ocana, E. Martínez-Enriquez, and S. Marcos, "OCT-based crystalline lens
687 topography in accommodating eyes," *Biomed Opt Express*, vol. 6, no. 12, pp. 5039-54, Dec 1 2015, doi:
688 10.1364/BOE.6.005039.

689 [11] K. Karnowski, B. J. Kaluzny, M. Szkulmowski, M. Gora, and M. Wojtkowski, "Corneal topography with
690 high-speed swept source OCT in clinical examination," *Biomed Opt Express*, vol. 2, no. 9, pp. 2709-20, Sep
691 1 2011, doi: 10.1364/BOE.2.002709.

692 [12] J. Fujimoto and D. Huang, "Foreword: 25 Years of Optical Coherence Tomography," *Investigative
693 Ophthalmology & Visual Science*, vol. 57, no. 9, pp. OCTi-OCTii, 2016, doi: 10.1167/iops.16-20269.

694 [13] D. Huang *et al.*, "Optical coherence tomography," *Science*, vol. 254, no. 5035, pp. 1178-81, Nov 22 1991,
695 doi: 10.1126/science.1957169.

696 [14] G. Muralidharan, E. Martínez-Enriquez, J. Birkenfeld, M. Velasco-Ocana, P. Pérez-Merino, and S. Marcos,
697 "Morphological changes of human crystalline lens in myopia," *Biomed. Opt. Express*, vol. 10, no. 12, pp.
698 6084-6095, 2019/12/01 2019, doi: 10.1364/BOE.10.006084.

699 [15] P. Pérez-Merino, M. Velasco-Ocana, E. Martínez-Enriquez, L. Revuelta, S. A. McFadden, and S. Marcos,
700 "Three-dimensional OCT based guinea pig eye model: relating morphology and optics," *Biomed. Opt.
701 Express*, vol. 8, no. 4, pp. 2173-2184, 2017/04/01 2017, doi: 10.1364/BOE.8.002173.

702 [16] Y. Yang, E. Pavlatos, W. Chamberlain, D. Huang, and Y. Li, "Keratoconus detection using OCT corneal
703 and epithelial thickness map parameters and patterns," *J Cataract Refract Surg*, vol. 47, no. 6, pp. 759-766,
704 Jun 1 2021, doi: 10.1097/j.jcrs.0000000000000498.

705 [17] S. Marcos *et al.*, "Simulating Outcomes of Cataract Surgery: Important Advances in Ophthalmology," *Annu
706 Rev Biomed Eng*, vol. 23, pp. 277-306, Jul 13 2021, doi: 10.1146/annurev-bioeng-082420-035827.

707 [18] E. Martínez-Enriquez, P. Pérez-Merino, S. Durán-Poveda, I. Jiménez-Alfaro, and S. Marcos, "Estimation
708 of intraocular lens position from full crystalline lens geometry: towards a new generation of intraocular lens
709 power calculation formulas," *Scientific Reports*, vol. 8, no. 1, p. 9829, 2018/06/29 2018, doi:
710 10.1038/s41598-018-28272-6.

711 [19] Y. S. Yoo *et al.*, "Use of the Crystalline Lens Equatorial Plane as a New Parameter for Predicting
712 Postoperative Intraocular Lens Position," (in eng), *Am J Ophthalmol*, vol. 198, pp. 17-24, Feb 2019, doi:
713 10.1016/j.ajo.2018.09.005.

714 [20] S. Norrby, "Sources of error in intraocular lens power calculation," *J Cataract Refract Surg*, vol. 34, no. 3,
715 pp. 368-76, Mar 2008, doi: 10.1016/j.jcrs.2007.10.031.

716 [21] S. Marcos, S. Ortiz, P. Perez-Merino, J. Birkenfeld, S. Duran, and I. Jimenez-Alfaro, "Three-dimensional
717 evaluation of accommodating intraocular lens shift and alignment in vivo," *Ophthalmology*, vol. 121, no. 1,
718 pp. 45-55, Jan 2014, doi: 10.1016/j.ophtha.2013.06.025.

719 [22] P. Perez-Merino *et al.*, "Aberrometry in patients implanted with accommodative intraocular lenses," *Am J
720 Ophthalmol*, vol. 157, no. 5, pp. 1077-89, May 2014, doi: 10.1016/j.ajo.2014.02.013.

721 [23] A. de Castro, P. Rosales, and S. Marcos, "Tilt and decentration of intraocular lenses in vivo from Purkinje
722 and Scheimpflug imaging. Validation study," *J Cataract Refract Surg*, vol. 33, no. 3, pp. 418-29, Mar 2007,
723 doi: 10.1016/j.jcrs.2006.10.054.

724 [24] M. Sun, A. de Castro, S. Ortiz, P. Perez-Merino, J. Birkenfeld, and S. Marcos, "Intraocular lens alignment
725 from an en face optical coherence tomography image Purkinje-like method," *Optical Engineering*, vol. 53,
726 no. 6, p. 061704, 2014. [Online]. Available: <https://doi.org/10.1117/1.OE.53.6.061704>.

727 [25] L. Wang, R. Guimaraes de Souza, M. P. Weikert, and D. D. Koch, "Evaluation of crystalline lens and
728 intraocular lens tilt using a swept-source optical coherence tomography biometer," *J Cataract Refract Surg*,
729 vol. 45, no. 1, pp. 35-40, Jan 2019, doi: 10.1016/j.jcrs.2018.08.025.

730 [26] N. Hirmschall, T. Buehren, F. Bajramovic, M. Trost, T. Teuber, and O. Findl, "Prediction of postoperative
731 intraocular lens tilt using swept-source optical coherence tomography," *J Cataract Refract Surg*, vol. 43,
732 no. 6, pp. 732-736, Jun 2017, doi: 10.1016/j.jcrs.2017.01.026.

733 [27] K. Waser *et al.*, "Predicting intraocular lens tilt using a machine learning concept," *J Cataract Refract Surg*,
734 vol. 50, no. 8, pp. 805-809, Aug 1 2024, doi: 10.1097/j.jcrs.0000000000001452.

735 [28] Q. Lu, W. He, D. Qian, Y. Lu, and X. Zhu, "Measurement of crystalline lens tilt in high myopic eyes before
736 cataract surgery using swept-source optical coherence tomography," *Eye and Vision*, vol. 7, no. 1, p. 14,
737 2020/03/06 2020, doi: 10.1186/s40662-020-00176-5.

738 [29] E. Martínez-Enriquez, M. Sun, M. Velasco-Ocana, J. Birkenfeld, P. Perez-Merino, and S. Marcos, "Optical
739 Coherence Tomography Based Estimates of Crystalline Lens Volume, Equatorial Diameter, and Plane
740 Position," *Invest Ophthalmol Vis Sci*, vol. 57, no. 9, pp. OCT600-10, Jul 1 2016, doi: 10.1167/iops.15-
741 18933.

- [30] E. Martínez-Enríquez, A. de Castro, and S. Marcos, "Eigenlenses: a new model for full crystalline lens shape representation and its applications," *Biomed Opt Express*, vol. 11, no. 10, pp. 5633-5649, Oct 1 2020, doi: 10.1364/BOE.397695.
- [31] E. Martínez-Enríquez *et al.*, "Estimation of the full shape of the crystalline lens in-vivo from OCT images using eigenlenses," *Biomed. Opt. Express*, vol. 14, no. 2, pp. 608-626, 2023/02/01 2023, doi: 10.1364/BOE.477557.
- [32] A. Akman, L. Asena, and S. G. Gungor, "Evaluation and comparison of the new swept source OCT-based IOLMaster 700 with the IOLMaster 500," *Br J Ophthalmol*, vol. 100, no. 9, pp. 1201-5, Sep 2016, doi: 10.1136/bjophthalmol-2015-307779.
- [33] A. Ruiz-Calvo, D. Ansah, U. Celik, S. MacRae, S. Marcos, and E. Martínez-Enríquez, "Automatic segmentation and quantification of OCT images before and after cataract surgery using deep learning," *Appl. Opt.*, vol. 63, no. 20, pp. 5376-5386, 2024/07/10 2024, doi: 10.1364/AO.524950.
- [34] S. Ortiz, D. Siedlecki, L. Remon, and S. Marcos, "Optical coherence tomography for quantitative surface topography," *Appl Opt*, vol. 48, no. 35, pp. 6708-15, Dec 10 2009, doi: 10.1364/AO.48.006708.
- [35] C. E. Rasmussen and C. K. I. Williams, *Gaussian Processes for Machine Learning (Adaptive Computation and Machine Learning)*. The MIT Press, 2005.
- [36] "Statistics and Machine Learning Toolbox™ User's Guide," *The MathWorks, Inc* 2024.
- [37] C. E. Rasmussen, "Gaussian Processes in Machine Learning," in *Advanced Lectures on Machine Learning: ML Summer Schools 2003, Canberra, Australia, February 2 - 14, 2003, Tübingen, Germany, August 4 - 16, 2003, Revised Lectures*, O. Bousquet, U. von Luxburg, and G. Rätsch Eds. Berlin, Heidelberg: Springer Berlin Heidelberg, 2004, pp. 63-71.
- [38] S. Marcos, P. Rosales, L. Llorente, S. Barbero, and I. Jiménez-Alfaro, "Balance of corneal horizontal coma by internal optics in eyes with intraocular artificial lenses: Evidence of a passive mechanism," *Vision Research*, vol. 48, no. 1, pp. 70-79, 2008/01/01/ 2008, doi: <https://doi.org/10.1016/j.visres.2007.10.016>.
- [39] E. Martínez-Enríquez *et al.*, "Estimation of the IOL position using the full shape of the crystalline lens and machine learning algorithms," *Investigative Ophthalmology & Visual Science*, vol. 65, no. 7, pp. 6326-6326, 2024.
- [40] "<https://github.com/EduardoMartinezEnriquez/Postoperative-intraocular-lens-tilt-from-preoperative-full-crystalline-lens-geometry>".